Proceedings of Enrico Fermi School
"Organic Nanostructures"
Varenna, Italy, July 2001

TUNABLE PHOTONIC NANOSTRUCTURES 2: SEMI-TRANSPARENT METALLIC OPAL REPLICAS AND NANOCOMPOSITES

A. A. Zakhidov[1], R. H.Baughman[1] I.I. Khayrullin[2], M.Kozlov[2] and I.Udod[2],
[1]*UTD-NanoTech Institute, University of Texas at Dallas, TX 75083, USA*
[2]*Honeywell Laboratories, Honeywell Intl., Morristown, NJ 07962, USA*

N. Eradat[+], J. D. Huang[*], A. Pokrovsky, A. Efros and Z. V. Vardeny,
Department of Physics, University of Utah, Salt Lake City, Utah 84112, USA

1. INTRODUCTION.

The same free electron plasma that causes usual metals to be conducting also causes them to be non-transmissive to electromagnetic waves. As well known at frequency (ω) below the plasma frequency (ω_p), the dielectric permitivity ($\varepsilon = 1 - (\omega_p/\omega)^2$) becomes negative and the refractive index ($n(\omega) = (\varepsilon\mu)^{1/2}$, where μ is the magnetic permeability) becomes imaginary. Therefore, electromagnetic waves can not effectively propagate inside metals, but are instead reflected for good metals and both reflected and absorbed for less conductive metals. This point emphasizes that high transparency (T) and high electrical conductivity (σ) are contradictory properties, and that the product $T\times\sigma$ can not be maximized in the usual bulk materials found in nature. The motivation of the present work was to create photonic crystals (PC), not of conventional dielectric type [1-2], but of metallic periodic nanostructures or metallo-dielectric nanocomposite PC in which $T\times\sigma$ can be maximized. Moreover optical and electronic properties can be maid tunable because of the utilization of geometry and topology of interpenetrating components separated by a large interfacial area A_v in a photonic crystal structure.

Why are such meta-materials needed for optoelectronic and photonic

[+]Present address: NP Photonics, University of Arizona Science and Technology park, 9030 S. Rita Rd., Suit 120, Tucson, Arizona 85750, USA
[*] Present address: E-tech, 1865 Lundy Avenue, San Jose, California 95131, USA

applications? Modern photonics and electronics technologies require good electronic conductors that are at the same time highly transparent. This need is becoming increasingly important, with the rapidly growing use of photonic telecommunication, optical data transfer between electronic chips, and the ultimate possibility of all-optical computers. The reversible transformation between photons and electrons employs photodetectors and lasers (particularly VCSELs), which both need materials that simultaneously have high electronic conductivity and high optical transmissivity. This need is further increased for novel optoelectronic devices targeted in the proposed research, in which interpenetrating electronically conductive and electro-optically responsive materials are combined in a three-dimensionally periodic meta-material structure.

1-D and 2-D Metallo-dielectric (M-D) nanostructures have been studied recently, and it has been found that incorporation of metals into ordered dielectric structures can significantly change their bulk optical properties [3-8,10-15]. So it has been found recently that the best mirrors, can be created not by bulk metals, but by the metallo-dielectric photonic crystals with sub-micron scale metallic spheres embedded into the dielectric body [5,11]. The losses are highly suppressed in such metallo-dielectric photonic crystal mirrors, which are omni-directional reflectors [11].

Several interesting phenomena have been found for 1-d [6,7]and 2-d [10,13] metallo-dielectric nanostructures. So in layered M-D systems the enhanced transmission of light, due to a sort of resonant photon tunneling from one metallic (M) layer to another in periodic M-D-M-D-multi-layered structures [6]. In this interesting phenomena transmission (T) can be unexpectedly high even if the total thickness of M layers is larger than skin depth. [6,7].

On the other hand if instead of layers there are M disks, patches of particles the wide stop bands are created by multiple scattering from separated metallic inclusions.

In all above phenomena the metallic inclusions are not connected to each other and so the electrical conductivity is either absent [8] or is high only along the metallic sheets direction [4,5]. The situation changes for the 3-D interconnected systems like wire meshes, which have been studied in microwave range, when size of periodicities is of

several cm, or mm. The electromagnetic properties of a 3-dimensional wire mesh in network type geometry resembling covalently bonded diamond has been studied experimentally in [10,14,15] for microwave region. The frequency and wave vector dispersion showed forbidden bands at the frequencies ωo, of dielectric PBG, corresponding to the lattice spacing, just as in dielectric photonic crystals PBG. But, they have also new forbidden band which starts at zero frequency and extends to a certain ω cut-off, acting as a type of plasma cut-off frequency of infinite metals. This band called as a metallicity gap is in fact not related with a periodicity, but with a metallicity, or the existence of free charge carriers [3,4].

To observe this gaps the size of fine mesh has been lowered till microns, but it was not possible till this present work to create large enough samples of fine metallic meshs at opt sub-micron length scales, suitable for optical studies.

It was not clear however how this metallic-PBG will appear in the optical wavelength scales of 100s of nm: because extending to sub-micron range creates not only technological problems but also brings uncertainty in physics of electromagnetic excitations in such fine nanostructures. The theory of metallicity PBG is not straight-forward here, like in case of microwaves or using simple scaling arguments, which are valid only for dielectric PBG systems, without account of dispersion of $\varepsilon(\omega)$. The interplay between strong dispersion of metals, $\varepsilon = 1 - (\omega_p^2/\omega(\omega+\iota\gamma)$ with absorption ($\sim \gamma$, due to finite conductivity) does not allow to make direct predictions, based on scaling arguments. So we address this problems here both experimentally and theoretically.

Highly periodic, three-dimensional metallic mesh nano-composites with silica spheres have been prepared by micro-molding synthetic opals using melts of metals and semimetals. These metallic photonic crystal nanostructures show photonic and electronic properties, which strongly depend on their geometry and topology. We observed dramatic differences in the reflectivity spectra of two topologically different metallic nano-structures, namely those with either network (continuous) or cermet (discontinuous) topologies. The plasmon derived reflection edge of conventional bulk metal is found to red shift to infrared region, due to dramatic change of the plasmon spectra in metallic nano-mesh, opening a semi-transparency window. Due to this window in the visible

spectral range bright colors of Bragg scattering can be observed from both topologies, which are more intense than in conventional, dielectric gem opals. Highly interconnected metallic photonic crystal structures showed about one order of magnitude decrease in the effective plasma frequency compared to that of the bulk metals, while in disconnected nano-composites the reflection edge shifts even much further into infrared. Coherent backscattering measurements showed a much larger optical mean free path for the metal-infiltrated opals compared to the skin depth of the metals, in agreement with the reduction in the plasma frequency. We also found an extra band in the reflectivity spectra of network-type samples that might be related to new branches of one-dimensional and surface plasmons in this topologically sophisticated metallic nanostructures. We thus demonstrated that reflectivity and hence transparency of metallic photonic crystal nano-structures can be tuned in a wide range by changing geometry (via filling factor) and topology (via connectivity).

In purely dielectric structures an optical PBG gap $\Delta\omega$ (shown at Fig. 8, (d)) opens up at the edge of the Brillouin Zone ($k=\pi/d$) that arises from interference of the foregoing and reflected electromagnetic waves inside the periodic structure. The gap center frequency, ω_o, is determined by the size of the reciprocal lattice, whereas the gap width is proportional to ω_o and dielectric constant contrast of the PBG constituents. In metallo-dielectric structures, however, depending on the topology, two cases are recognized as is shown below.

(a) As in the dielectric counterparts, in metallic network structures narrow forbidden gaps are observed at ω_o that corresponds to the spatial periodicity of the structure. By far the most dominant feature of the metallic mesh structure, however was a strong three-dimensional stop band starting from zero frequency up to a finite frequency, $\tilde{\omega}_p$, that may be due to a diluted plasma wave associated with the electrons' motion in the interconnected wire network. It might be considered as a three-dimensional cut off frequency [3]. We will show that in our system the metallicity gap is actually very narrow, namely due to existence of very slow 1-d plasmon branches starting from zero frequency (see theory below and in [20]).

(b) In cermet-type topology the band structure resembles that of the more

conventional dielectric/air photonic crystals, where the EM waves are concentrated within the dielectric phase. However, for smaller separation of the islands, the nature of the band structure changes by strong capacitive interaction between the metallic inclusions that leads to an increase in the Bragg-derived gap width [6].

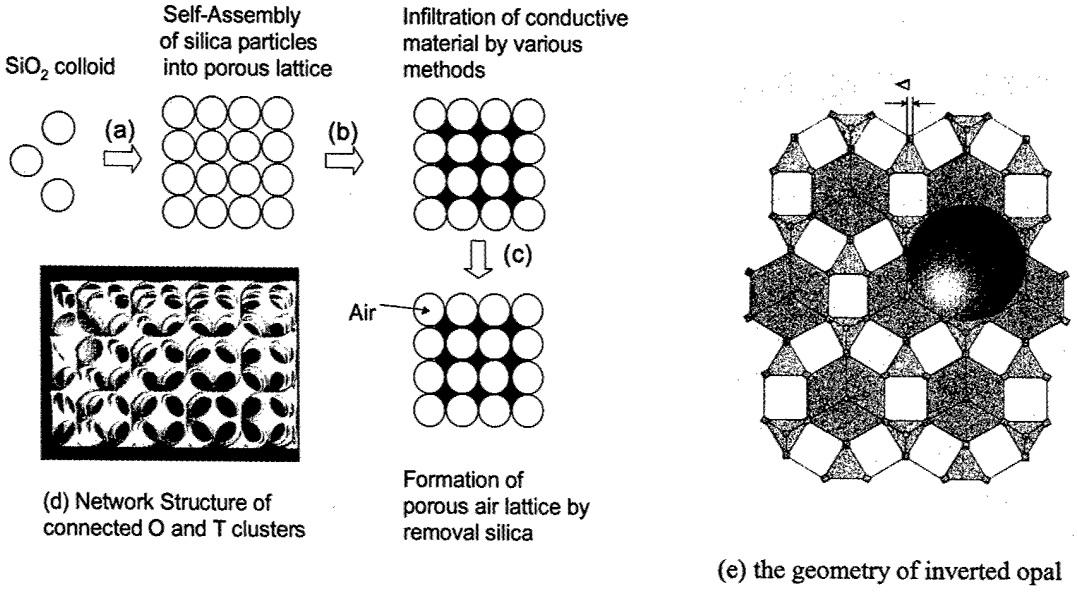

Figure 1. The schematics of the process of opal templating for preparation of inverted opal metallic photonic crystals with sub-micron periodicities. (a): the fcc porous lattice of silica opal is first crystallized by self-assembly of mono-dispersed SiO_2 spheres in the range of 150-400 nm and then sintered at high temperature; (b) the metal melt is infiltrated under high pressure and solidified at either the same pressure or at lower pressure. At this step the metallo-dielectric 3-D nano-composite is obtained; (c) The host silica can be removed, leaving an inverted opal replica lattice; (d) computer model of the network topology of inverted lattice showing each octahedral void (O) connected with 8 tetrahedral (T) voids via narrow necks. e) The tetrahedral and octahedral voids of the opal matrix are connected with each other through 100 to 500 Å diameter thin necks with the diameter of $\Delta = (2/3^{1/2})$ d-D, in the ideal case.

In this work we demonstrate the dramatic changes in the reflectivity spectra of metal-infiltrated opals when changing from cermet to network topologies, and particularly in metallic mesh structures formed after dissolving the SiO_2 spheres. We found a substantial red shift in the cut-off frequency, $\tilde{\omega}_p$, of network-type metal-infiltrated opals [of the type in Fig. 1(c)]; this defines a complete metallicity gap. We

found that $\tilde{\omega}_p$ depends on the filling factor of the metallic element in the binary structure. Moreover, we also observed an additional incomplete gap that opens at higher frequencies. This gap is more pronounced in metallic replicas [of Fig. 1(d) and Fig.2. a) and b)] and may be related to various plasma (surface and 1-d plasmon) modes of the network. A theoretical model has been formulated to explain the reported experimental observations [20].

FABRICATION OF METALLIC NANOSTRUCTURES

Self-assembled PBG structures such as silica opals and other fcc colloidal crystals have many advantages for photonic PBG-nanotechnology [22-32], i.e. for fabrication of various nanostructures, based on templating fcc lattices of porous opals. These structures show incomplete stop-bands in the visible range of the EM spectrum, [22-24]). Opals are close-packed face-centered cubic sediments formed from aqueous suspensions of mono-dispersed silica (SiO_2) spheres [**Fig. 1(a)**]. Although calculations revealed that it is not possible to form a complete PBG in uninfiltrated opal [11], but nevertheless in studies of photonic crystals the structure serves as the first solid three-dimensional PBG crystal with incomplete gaps in certain directions in the visible spectral range. Recently, different groups have used SiO_2, polystyrene, and PMMA opals as templates for fabricating inverse PBG structures. Such inverse PBG crystals are made of inorganic oxides [22], polymers [23, 26], diamond and glassy carbon [23], semiconductor quantum dots [24], and gold [25,26]. Excellent overview of recent advances is given in [33].

We have recently developed a simple method to fabricate 3-D composite superstructures by using porous synthetic opals as templates (Fig. 1) [23,32]. Similar methods can be used for processing metals and semiconductors into more complex geometries as compared to carbon inverted opal [21]. By manipulating the wetting conditions and size of the interconnects between various voids in the opal, we could create a 3-D porous metal or semiconductor with either continuous or discontinuous mesh structures having periodic breaks between clusters in the opal voids. Provided such tructures are fabricated, they would possess interesting photonic and electron transport properties due to possible light localization and confinement phenomena, since the large

tetrahedral and octahedral voids of the opal matrix are connected with each other through 100 to 500 Å diameter thin necks.

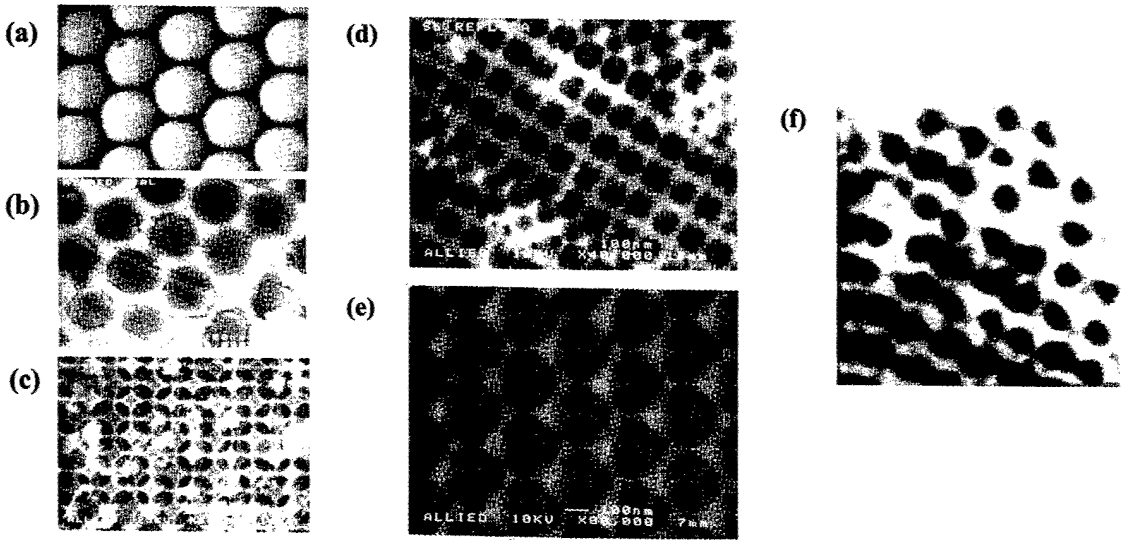

Fig. 2. Images of various metallic nanostructures obbtained by micromolding and templating: (a) initial porous SiO_2 opal mattrix, (b) Bi-infiltrated silica opal, (c) Sb-inverted opal replica after dissolving silica (the brakes between octahedral clusters are clearly seen), (d) Sb-replica with larger filling factor f and thus smaller number of brakes, (e) Bi-Te high fidelity replica with thin interconnects, (f) the cermet topology of metallo-dielectric nanocomposite of Sb-silica obtained by remelting.

Molten metal infiltration. The conductors that were infiltrated into opal were either metals (Sn, Pb, and Sb), semimetals (In, Bi, and Te) or their alloys (Bi_xSb_y and Bi_xTe_y). For simplicity we refer to all of them as metals and the product obtained upon filling the opal matrix with these metals as metal infiltrated opal. In a typical preparation process, a rectangular piece of opal (with average size $5\times5\times5$ mm^3) was surrounded with metallic powder that tightly filled a 9 mm diameter stainless steel cylinder using a piston-cylinder pressure cell. This cylinder was held at 100-650°C under pressure of 1 kbar to 10 kbar for 10 min to 2 hours. During this period of time, the melt entirely filled the void space available through the interconnecting channels. The pressure was lowered during solidification and then was completely released, once the piston-cylinder was cooled

down to ambient temperature. The infiltrated opal sample was then carefully cut from the surrounding pure metal using a jeweler's saw and polished. An average metal infiltrated opal sample obtained in this way had a cross-section of 5×5 mm^2 and thickness of 2 mm to 5 mm . Topology of the infiltrated material inside the voids of opal depends on the wetting between infiltrated material and silica and the amount of pressure applied during the infiltration process. When the wetting is poor or there is not enough pressure the sample acquires cermet-type topology Fig.2,a). Applying higher pressure in presence of adequate wetting results in a network type topology of metal-silica nanocomposite. To obtain metallic hollow replica we place the sample in HF to dissolve silica, and obtained high fidelity metallic meshes with geometry (see Fig.2, c,d,e,) depending on preparation conditions and sintering level of initial template. For more detailed information on the fabrication and characterization of the porous synthetic opal and infiltration process see ref. 21. Also the details on Measurement Apparatus are given in ref. [18] and [19].

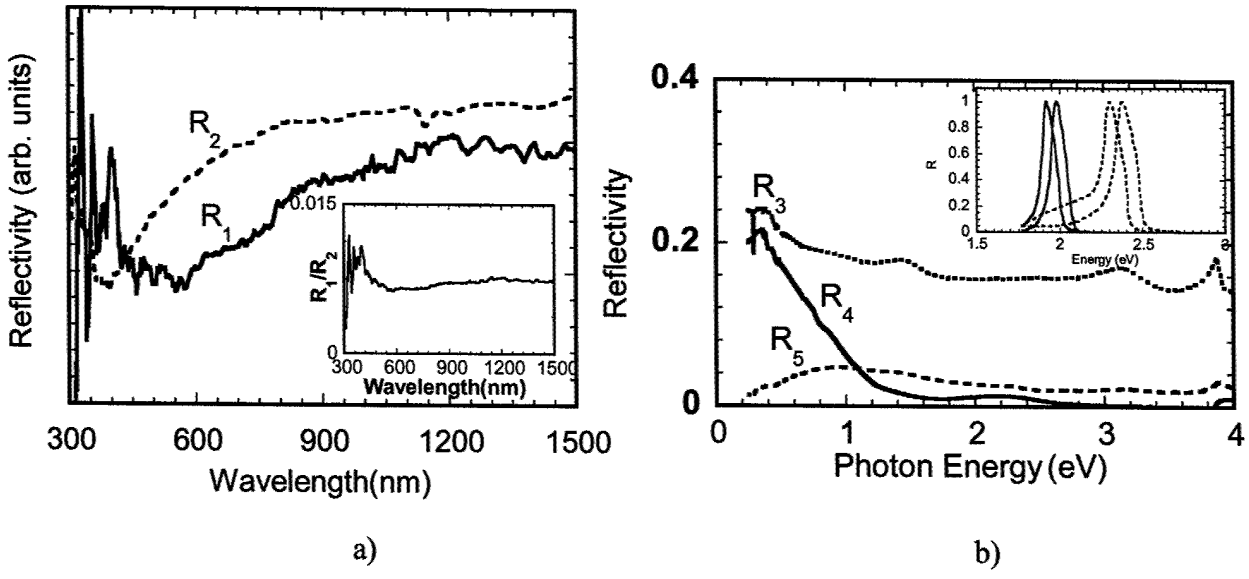

Figure 3. a) Reflectivity spectra of mercury infiltrated opal, R_1, and liquid mercury, R_2. The inset shows the relative reflectivity spectrum R_1/R_2. b) Specular reflectivity spectra of Sb, R_3, Sb infiltrated in "red" opal, R_4, and Sb infiltrated in "green" opal, R_5 compared

to reflectivity spectrum of Sb replica R_6.The "green" sample does not conduct (cermet topology) whereas the "red" sample is a conductor (network topology). The inset shows the Bragg peaks from the "red" (solid lines) and the "green" (dash lines) samples at 5 and 10 degrees inclination angles respect to [111].

RESULTS AND DISCUSSION

Two sets of cermet-type and network-type samples were identified by their conductivity, where cermet-type samples do not conduct. More important are the differences that we discovered in their optical properties, which are related to their transport properties. As described below, we found that all samples show Bragg stop bands in the visible spectral range. These bands are due to the periodicity of the underlying structure and are sensitive to the impinging angle of the light beam. On the other hand the specular, reflectivity spectra from the polycrystalline sample have not shown any dramatic change with the impinging angle. In addition, in order to observe a possible plasma frequency shift in the metallic PBG structures, we compared the reflectivity spectra of the metal-infiltrated opal samples with those of the same metals in bulk form.

In **Fig. 3, a)** we plot the reflectivity spectrum, R_1, of mercury (Hg) infiltrated opal compared to that of liquid mercury, R_2.The inset shows the relative reflectivity spectrum R_1/R_2 that is almost flat. Due to poor wetting between mercury and silica, the mercury chunks that infiltrate into the opal voids are disconnected. We could not confirm this assumption by SEM since mercury would evaporate into the vacuum chamber. However conductivity measurements indicated that the mercury inclusions in the opal are indeed disconnected. From here on we will assign color to the opal samples based on the maximum Bragg stop band wavelength that is determined by the diameter of the silica balls and the amount of sintering. The reflectivity spectra of bulk antimony (Sb), R_3, Sb infiltrated into "red" opal, R_4, and into "green" opal, R_5, are respectively presented in **Fig. 3, b)**. Angle-dependent Bragg peaks at 5^0 and 10^0 are also plotted in the inset as solid and dashed lines for red and green samples, respectively. Based on the light penetration depth, δ, in the bulk form of the metals used in our samples (δ<15nm) we would not expect to

see any Bragg reflection from these samples. However due to enhanced EM transmission [9], which is caused as we believe (see theory below) by the lower cut-off frequency, $\tilde{\omega}_p$ inside the opals, the light penetrates many layers into the metallic PBG samples (which is not normally possible beyond the skin depth for light with $\omega < \omega_p$ for bulk metals in which bulk plasmon ω_p is much higher than ω of visible light) and as a result Bragg peaks can be formed in backscattered light. Preliminary measurements of coherent backscattering from a metallic PBG sample (Sb-infiltrated red opal) showed a mean free path of ~1.5 μm, proving that a longer light-penetration depth exists in the metal infiltrated opals [19] compared to the metal skin depths.

Whereas the angle-resolved Bragg peaks show similar behavior in both Sb samples, the specular reflectivity spectra have major differences. The reflectivity spectrum of the "red" Sb-opal sample is almost negligible in the spectral range, $\hbar\omega$, of 1.3 to 4 eV but abruptly increases at lower $\hbar\omega$. The reflectivity of the "green" Sb-opal, on the contrary, goes to zero at lower $\hbar\omega$. Moreover when measuring conductivity we observed that the "red" Sb sample was conducting, whereas the "green" Sb sample was not. We thus conjecture that the "red" Sb-opal sample has a network-type topology with shifted cut-off frequency, whereas the "green" Sb-opal sample has a cermet-type topology just due to smaller voids for metal filling (details in [18,21]). It is worthwhile mentioning that the formation of cermet- and network-type topologies not only depends on the wetting properties of the infiltrated metals but also on the infiltration parameters, such as temperature, pressure, and the amount of sintering that determines the size of the interconnecting channels. The silica sphere size, however is not an essential parameter. After dissolving away the silica spheres in the "red" opal sample, a Sb replica structure was formed. This structure is a metallic mesh filled with air spheres [**Fig. 1(d)** and **Fig. 2, (c), (d)**]. The Bragg peaks observed from this structure are even brighter [**Fig. 4(b)** and inset **of Fig 8**].

We also measured the specular reflectivity R_6, from Sb bulk, and R_7, from the Sb replica. We again observed a red shifted cut off frequency [**Fig. 4(a)**] for the metallic replica. However we found that there is an additional reflectivity band in the visible

spectral range [**Fig. 4(a)**] for both metal infiltrated opal and metallic replica, where it is more pronounced in the replica sample. This band appears at frequencies higher than the new cut-off frequency of the metallic mesh, $\tilde{\omega}_p$ and does not shift with the impinging angle (R_{12}, R_{13}, R_{14} at $\theta=5^0$, 15^0, 25^0 respectively) [**Fig. 4(b)**], as is the case for the Bragg bands

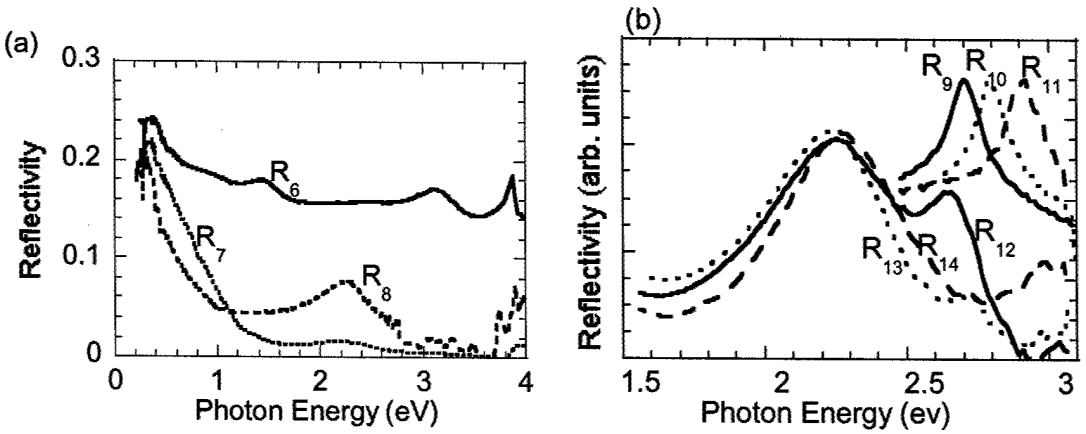

Figure 4 (a) Specular reflectivity spectra of Sb, R_6, Sb infiltrated in "red" opal, R_7, and Sb replica, R_8. Both PBG samples are conductors (network topology). Notice the reflectivity band at. 2.2 eV in both R_5 and R_6 spectra related to the surface plasmons. (b) The Bragg peaks (R_9, R_{10}, R_{11}) and the plasmon peaks (R_{12}, R_{13}, R_{14}) from the Sb replica sample at 5, 15, and 25 degrees inclination angle respect to the [111] direction. Note that the surface plasmon band does not have the same angle dependence as that of the Bragg bands. The peaks above 2.5 eV in R_{12}, R_{13}, R_{14} are related to the Bragg reflection from the (220) crystallographic planes. Notice the angular dispersion of these peaks.

(R_9, R_{10}, R_{11} at $\theta=5^0$, 15^0, 25^0 respectively). Theoretical calculations show that the reflectivity peak in the visible spectral range is related to surface plasmons that do not depend on the filling factor of the metallic element. Similar results were obtained for opals having different periodicity when infiltrated with a variety of metals such as Sn, Bi, Bi-Sb, and Pb. In all cases we found that there is a good agreement between the transport (in sense of connectivity or cermet topology) and optical measurements.

Theory of plasmons in metallic nanocomposites.

Let us consider a system of infinite metallic wires of circular cross section, which form the cubic mesh, and embedded in a dielectric with a dielectric constant ε_m. We are going to consider the case when condition $\omega\tau << 1$ is fulfilled, where τ is an electron relaxation time in the metal. In this case we have a dispersion of the dielectric constant of the metal.

Dielectric properties of this system of wires described by the dielectric tensor, which can be written in the principal axes (the axes of cubic crystal) in the following form:

$$\begin{bmatrix} \varepsilon(\omega,k_y,k_z,k_x) & 0 & 0 \\ 0 & \varepsilon(\omega,k_z,k_x,k_y) & 0 \\ 0 & 0 & \varepsilon(\omega,k_x,k_y,k_z) \end{bmatrix}$$

where

$$\varepsilon(\omega,k_x,k_y,k_z) = \varepsilon_m - \frac{f}{3}\frac{\omega_p^2}{\omega^2 - \Omega^2(k_x,k_y,k_z)} - \frac{4f}{3}\varepsilon_m \frac{(\varepsilon_m - 1)\omega^2 + \omega_p^2}{(\varepsilon_m + 1)\omega^2 - \omega_p^2}$$

$$\Omega^2(k_x,k_y,k_z) = \Omega_0^2(k_x,k_y,k_z) - \frac{f}{\varepsilon_m}\omega_p^2 \frac{k_z^2}{k_x^2 + k_y^2 + k_z^2}$$

$\Omega_0^2(k_x,k_y,k_z)$ - plasma frequency of the whole system,

ω_p^2 - plasma frequency of the bulk metal of the nano-wires,

(k_x,k_y,k_z) - components of the wave vector,

f - volume fraction of the metal in the system (filling factor),

d - distance between the wires,

The difference of the $\Omega(k_x,k_y,k_z)$ in the dielectric constant from the $\Omega_0^2(k_x,k_y,k_z)$ is because of the difference of the average electric field from the acting electric field. In the limit $k_z d >> 1$ plasma frequency of the system Ω_0 has a form of a standard one dimensional plasmon.

In the general case, we have anisotropy of dielectric properties due to spatial dispersion. However if the wave vector has a [111] direction, then the dielectric tensor becomes a scalar $\varepsilon(\omega,k_x,k_y,k_z)$ (see Fig. 5).

Complete plasmon spectrum of the system is presented schematically on the Fig. 5,b). The lower branch corresponds to a one dimensional plasmon, ω_1 - is renormalized by the square root of the filling factor bulk plasmon, due to the part of dielectric constant which comes from metallic wires parallel to electric field vector ω_2 - is the surface plasmon, ω_3 - bulk plasmon. Both ω_2 and ω_3 come from the part of the dielectric constant which is due to the wires perpendicular to the electric field.

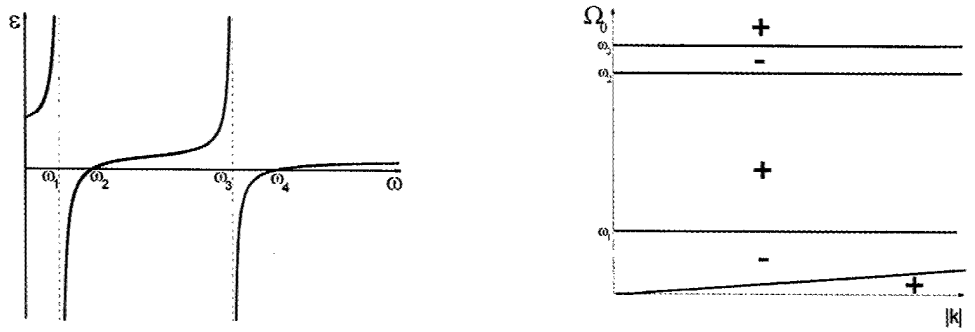

a) b)

Figure 5: a) Dispersion of the dielectric constant ε at a fixed value of the wave vector.

$$\omega_1 = \Omega(k_x, k_y, k_z),\ \omega_2 = \sqrt{\Omega^2(k_x, k_y, k_z) + f\omega_p^2/3\varepsilon_m},\ \omega_3 = \omega_p/\sqrt{\varepsilon_m + 1},$$

$$\omega_4 = \omega_3\left(1 + \frac{f}{6}(\varepsilon_m + 1)\right)$$

b. Plasmon spectrum of the system for the wave vector in [111] direction. The signs $\pm$ correspond to the sign of the dielectric constant ε.

$$\omega_1 = \sqrt{f\omega_p^2/3\varepsilon_m},\ \omega_2 = \omega_p/\sqrt{\varepsilon_m + 1},\ \omega_3 = \omega_2\left(1 + \frac{f}{6}(\varepsilon_m + 1)\right)$$

Using these dielectric properties of the system one can calculate the spectrum of electromagnetic waves in the system (see Fig. 6). The spectrum has a narrow gap between ω_2 and ω_3, which has a width proportional to the filling factor *f*. This is the only absolute gap which exists at all values of the wave vector ***k***. Another interesting property of the system is appearance of the double refraction (2 lower branches). It should be noted that the spectrum of these two waves depends on the wave vector ***k***, and double refraction

disappears at some particular directions (for example [111]). The upper branch of the spectrum asymptotically tends to the photon-like dispersion $ck/\sqrt{\varepsilon_m} = \omega$.

To compare with experimental data the reflection coefficient was calculated (see Fig. 4, 5). The peak in the reflection corresponds to the gap in the spectrum of electromagnetic excitations. On the experimental plots one can see a saturation of reflectivity at small frequencies. To explain this behavior we should propose that metallic wires in a real system have a finite length of the order of few microns and their lengths are randomly distributed. This gives the minimum value of $\boldsymbol{k}$ and therefore we get saturation of the reflection coefficient.

Reflection, transmission and absorption coefficients for the plate of the width of $h = 0.1\ mm$ are plotted on the Fig. 6.

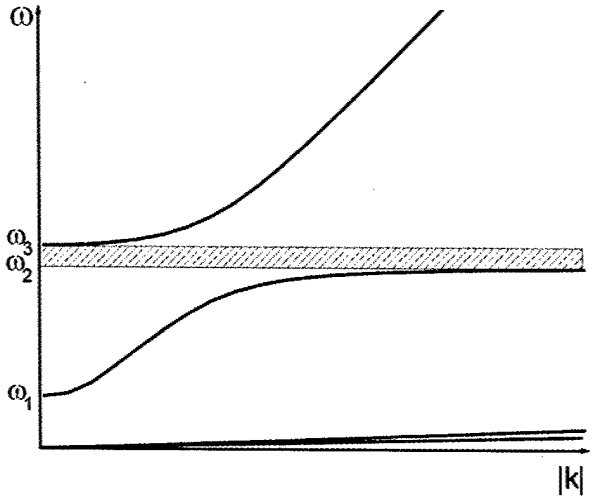

Fig. 6: Electromagnetic spectrum of excitations in metallic network of 3-D nanostructure system.

$$\omega_1 = \sqrt{f\omega_p^2/3\varepsilon_m}\ ,\ \omega_2 = \omega_p/\sqrt{\varepsilon_m + 1}\ , \omega_3 = \omega_2\left(1 + \frac{f}{6}(\varepsilon_m + 1)\right)$$

SUMMARY AND CONCLUSIONS.

We measured reflectivity spectra of several metallic PBG structures. We observed

Bragg stop bands in the visible spectral range and metallicity gap at $\tilde{\omega}_p < \omega_p$ in metallic PBG structures with a network topology. We found that the spectral range at which the metallicity gap opens depends on the lattice parameters and filling factor of the metallic components. In addition, we also observed a new reflectivity band in the visible spectral range that is related to the surface plasmons of these metallic mesh structures; it is more pronounced in metallic replicas. The position of this optical gap in the visible depends very weakly on the filling factor or impinging angle of the light beam. It roughly occurs at

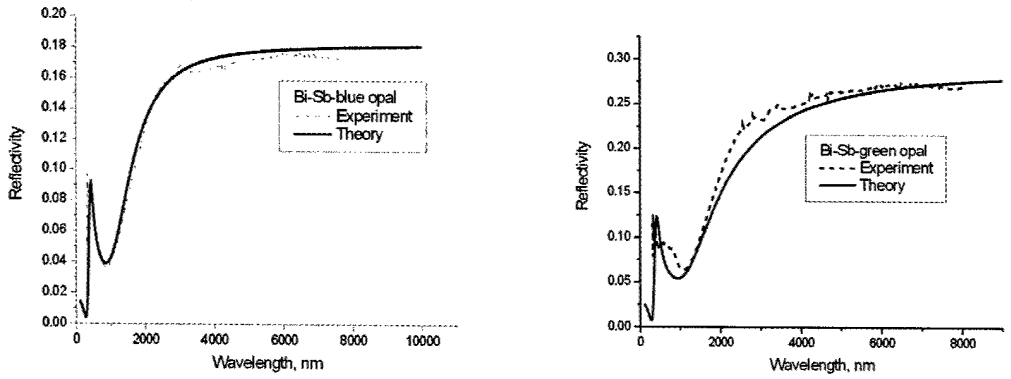

a) b)

Figure 7: Reflection spectrum for a) Bi-Sb blue opal nanocomposite (180 nm), b) Bi-Sb green opal (240 nm spheres)

$\omega_p/(\varepsilon_r+1)^{1/2}$, where ω_p is slightly modified plasma frequency of the bulk. This results allow to give some predictions on the optimal conditions for making metallic nanostructures, with maximized electrical conductivity and optical transparency.

The concept of highly transparent and conductive metallic nanostructures can be qualitatively understood using the diagram in Fig.8. Moreover, the viability of this concept is evident by comparing the quite different optical reflectivity of usual metals (Fig.8,a) with those we have observed in our metallic photonic crystals. Good metals have negative $\varepsilon<0$ below the plasma frequency ω_p, which is typically in the ultraviolet, so they reflect photons with $\omega < \omega_p$. In order to achieve high conductivity, high transparency and high internal surface area, one should fabricate network type metallic inverted opal

nanostructures, or in other words with much lower losses, that we have observed and assigned to the brakes in our metallic nanowires.

Because of the high porosity of these 3D metallic PCs having a percolated metal network topology, the concentration of electrons in the electron gas will be effectively diluted, while at the same time the connectivity of the metal network should be kept much higher (than we had in our nanocomposites) at significantly low filling factor of metal (ff < 0.2), which will insures a high σ. The consequence of this decrease in effective electron concentration at low ff is a shift of the transparency window from the ultraviolet to infrared or visible wavelengths. Due to the periodicity of our nanocomposites, reflectivity resonances should appear at wavelengths corresponding to the Bragg

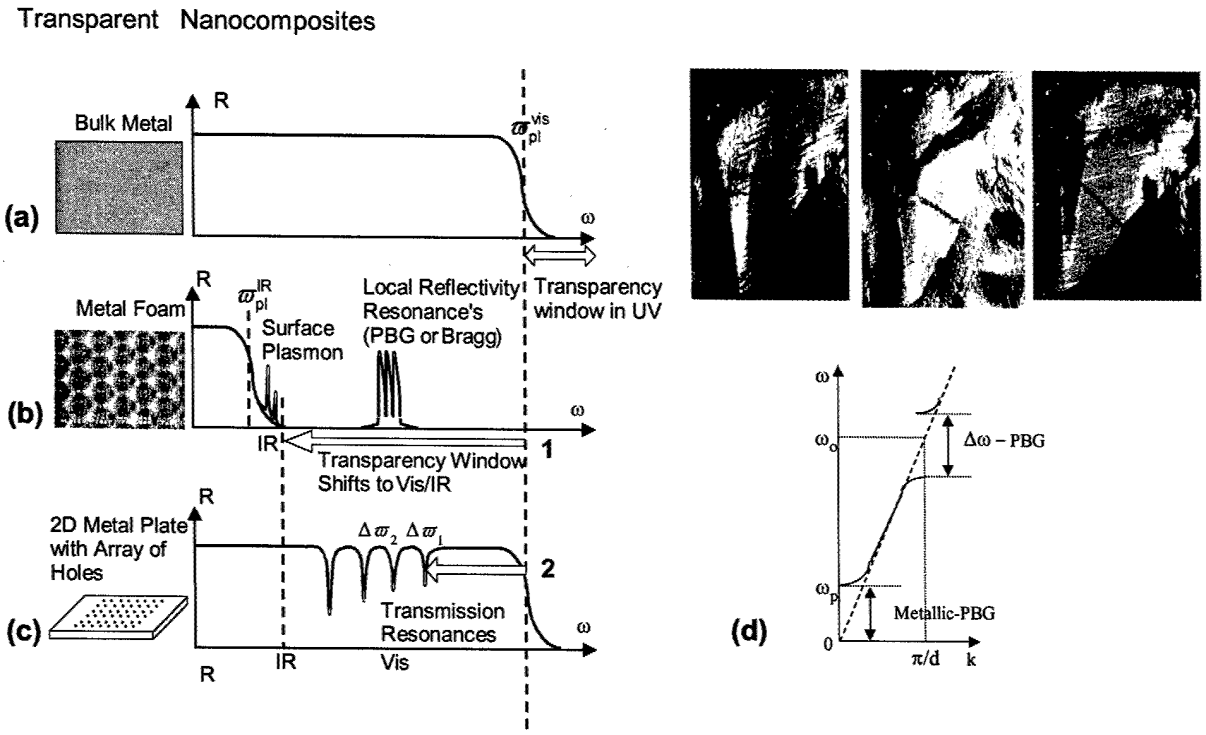

Figure 8. The diagram showing the expected reflectivity of electrically conductive nanostructures that becomes semi-transparent to electromagnetic radiation frequencies. (a) Typical reflectivity (R) spectrum of a bulk metal. Two approaches are illustrated for creating transparency windows in VIS/IR and MW regions: (b) using highly porous metallic 3-D nano-

foams or metallo-dielectric nanocomposites (described in present work), (c) sub-micron holes in metallic thin films (as demonstrated in [ ]). (d) schematic energy diagram showing dielectric type band gap and metallicity PBG below cut-off frrequency. The inset shows the observed bright Bragg colors of semi-transparent metallic Sb-inverted opals.

conditions, which are similar to dielectric PBGs, but might have different shapes and attenuation properties, i.e. intensity due to absorption in metals with finite conductivity . In Fig. 8, b, these Bragg-type resonances are shown as narrow peaks in the transparency window, opened in visible. The inset to Fig. 8 shows the actual image colorful of metallic nano-mesh of Sb in the reflected white light: it is a mirror with high metallic type reflectivity, but it is a color mirror, which changes a color depending on the incident angle. (see Fig. 4, b) Also, we have shown theoretically [20] and proven experimentally [18-19] that novel type of resonances can appear at the new plasmon edge, due to new types of plasmon excitations: both 1-D and 2-D surface plasmons in our three-dimensionally periodic meshes will be contributing to the resulting spectrum.

It should be noted that the plasmon resonances studied here in metallic nanostructures, are different from the transmission resonances recently found in thin metallic plates with periodic arrays of sub-micron holes [9]. Later phenomena schematically shown at Fig. 3 d) is also used to create transparency of metallic plates, but in much narower spectral bands.

Summarizing we show below the calculated transmission curve for metallic 3-D nano-wired mesh, with still significant absorption due to finite conductivity of the bulk metal of nano-wires and also due to existence of brakes in nano-wires. To increase the transmission at still high conductivity one should use metals with initially high bulk conductivity (i.e. Au or Ag, instead of Bi, or Sb studied here) and create nanostructures with much smaller number of brakes in the network of "wires" of metallic nanostructures.

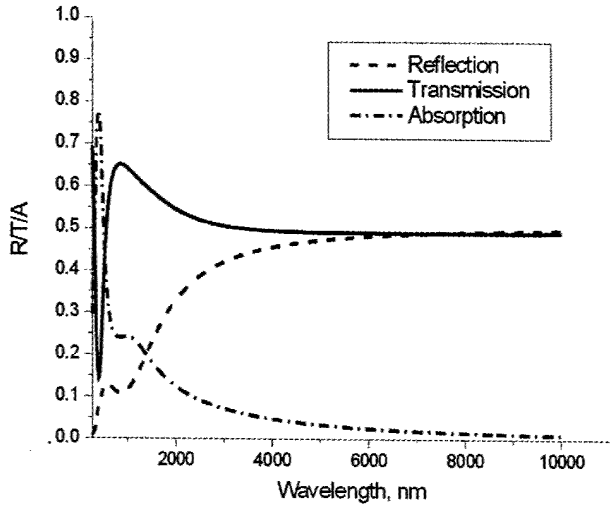

Figure 9: Calculated transmission, absorption and reflection from the plate of 0.1 mm width plate of metallic nano-mesh with finite absorption.

One other interesting possibility to increase conductivity at high transmissivity is to create the metallic opal, made of fcc lattice of metallic spheres, similar to one we have recently created [31].

ACKNOWLEDGMENTS

This work was supported in part by DARPA grant on "Advanced Nanostructured Thermoelectrics" and U. S. Army Research Office under DAAD19-99-1-0316.

REFERENCES

[1] YABLONOVITCH E., *Phys. Rev. Lett.* **58** (1987) 2059, JOHN S., Phys. Rev. Lett. **58** (1987) 2486.
[2] For review see JOANNOPOULOS J. D, MEADE R., WINN J.N, *Photonic Crystals*. (Princeton Press, Princeton) 1995 and articles in Photonic Band Gaps and Localization,
Vol **38** (1993) & **315** (1996) NATO ASI series, edited by C. M. Soukoulis, *Journal of the Optical Society of America,* B Vol. 10 (1993).
[3] MARADUDIN A. A., MCGURN A.R, *Phys.Rev.*, B **48** (1993) 17576.
[4] SIEVENPIPER M. E., SICKMILLER E., YABLONOVITCH J.N., in NATO ASI Ser., Ser. E., (1996), 315 (Photonic Band Gap Materials), 165-171.
[5] SCALORA M.; BLOEMER M. J.; BOWDEN C. M., Metals under a new light. *Opt. Photonics News,* **10(9)** (1999) 24-27.

[6] SCALORA M., BLOEMER M. J., PETHEL A.S., DOWLING J. P., BOWDEN C.M., MANKA A.S., *J.Appl.Phys.*, **83(5)** (1998) 2377-2383.
[7] SIBILIA C., SCALORA M., CENTINI M., BERTOLOTTI M., BLOEMER M. J., BOWDEN C. M., *J. Opt. A: Pure Appl. Opt.*, **1(4)** (1999) 490-494.
[8] SIEVENPIPER M. E., SICKMILLER E., YABLONOVITCH J.N., WINN S., FAN P.R., VILLENEUVE, JOANNOPOULOS J.D, *Phys.Rev.Lett.*, **80** (1998) 2829-2832.
[9] EBESSEN T.W., LEZEC H. J., GHAEMI H. F., THIO T., AND P.A. WOLFF, *Nature*, 391 (1998) 667-669.
[10] BROWN E.R., MCMAHON O.B., *Appl.Physics Letters*, (1995) 67 (15) 2138-40.
[11] SHANHUI F., VILENEUVE P.R., JOANNOPOULOS J. D., *Phys. Rev. B: Condens. Matter,* 54(16) (1996).
[12] GUPTA S., TUTTLE G., SIGALAS M. AND HO K. M, *Mat.Res. Symp. Proc.*, Vol. 484 (1998) 183-188.
[13] GUPTA S., TUTTLE G., SIGALAS M. AND HO K. M, *Appl.Phys. Lett.*, **71** (1997) 2412.
[14] SIGALAS M. M., BISWAS R., HO, K. M., SOUKOULIS C. M., CROUCH D. D., *Phys. Rev. B: Condens. Matter Mater. Phys.*, **60(7)** (1999) 4426-4429.
[15] PENDRY J. B., HOLDEN A. J., ROBBINS D. J. AND STEWART W. J, *J.Phys.:Condens. Matter,* **10** (1998) 4785-4809.
[16] Our experimental setup for measuring angle dependence of the Bragg peak consists of a Tungsten Halogen light source focused on the sample by a concave mirror. To accumulate a reasonable amount of light on the sample, we used a concave mirror with a diameter of 5cm and focal length of 60cm. This gave us beam divergence less than 5°. If we were to measure width of the peak we would have need parallel beam, but our goal was to determine the Bragg peak shift with illumination angle. Nonparallel beam would not change position of the peak though it will make the peak appear wider. The incident light was chopped at a frequency of 2KHz. We mounted the sample on a goniometer, which gave us ability to rotate the sample around three perpendicular axes. Having the sample mounted on the goniometer we get the diffracted light from a certain crystallite on the accumulating mirror. Focal point of accumulating mirror was set to be the at entrance slit of our spectrometer. An UV enhanced silicon detector was located at the exit of the spectrometer. The signal was amplified with a preamplifier and then guided to a lock-in amplifier. Reference signal came from the chopper that chops incident light before hitting the sample. Both the spectrometer and the lock-in amplifier were interfaced to a PC for data accusation. An extra flat mirror between the second concave mirror and the spectrometer allowed us to change angle of illumination and detection without having to move the spectrometer.

[17] ECONOMOU E. N., SIGALAS M. M., *Phys. Rev.*, B **48** (1993) 13434.
[18] ERADAT N., HUANG J. D., VARDENY Z. V., ZAKHIDOV A. A., BAUGHMAN R. H., *Synthetic Metals* **116**(2001)501
[19] HUANG J., RAIKH M. E., ERADAT N., VARDENY Z. V., ZAKHIDOV A. A., BAUGHMAN R. H., *Synthetic Metals* **116**(2001) 506
[20] POKROVSKY A., EFROS A., *Phys.Rev.B* (in press)
[21] ZAKHIDOV A. A., BAUGHMAN R. H, KHAYRULLIN I. I, UDOD I., KOZLOV M., ERADAT N., VARDENY V. Z., SIGALAS M., BISWAS R., *Synthetic Metals* **116**(2001)419.
[22] BOGOMOLOV V. N., *et al.*, *Phys. Rev.*, E **55** (1997) 7619.
[23] a) ZAKHIDOV A. A., BAUGHMAN R. H., IQBAL Z., CUI C., KHAYRULLIN I. I., DANTAS S.O., MARTI J., AND RALCHENKO V.G., *Science,* **282** (1998) 897.
b) YOSHINO K., TADA K., OZAKI M., *et al.*, *Jpn. J. Appl. Phys.*, **2** (1997) L714.

[24] VLASOV Y. A, ASTRATOV V. N., KARIMOV O. Z, KAPLYANSKII A. A., BOGOMOLOV V. N., PROKOFIEWV A. V., *Phys. Rev.*, B **55** (1997) R13357.
[25] VELEV O. D., *et al.*, *Nature,* **389** (1997) 447.
[26] IMHOF A., PINE D. J., *Nature,* **380** (1997) 948.
[27] PARKS S. H., XIA Y. N., *Chem. Matter*, **10** (1998) 1745.
[28] JOHNSON S. A., OLLIVIER P. J., MALLOUK T. E., *Science,* **283** (1999) 963.
[29] VLASOV Y. A., YAO N., NORRIS D. J., *Adv. Matter*, **11** (1999) 165.
[30] VELEV D. J., TESSIER P. M., LENHOFF A. M., KALER E. W., *Nature,* **401** (1999) 548.
[31] XU L, ZHOU W, KOZLOV M.E., KHAYRULLIN I.I, UDOD I, ZAKHIDOV A.A., BAUGHMAN R.H., AND WILEY J.B., *J. Am. Chem. Soc.* 123(2001) 763
[32] ZAKHIDOV A. A., BAUGHMAN R. H., CUI C., KHAYRULLIN I. I., LIU L. M., UDOD I., JI SU, KOZLOV M., *"Three Dimensionally Periodic Structural Assemblies on Nanometer and Longer Scales"* Patent Disclosure No. 30-464216.
[33] Review articles in special issue of *Advanced Materials* July (2001)